9 Recurrent Quantum Neural Network and its Applications

Laxmidhar Behera, Indrani Kar, and Avshalom C. Elitzur

Summary. Although the biological body consists of many individual parts or agents, our experience is holistic. We suggest that *collective response behavior* is a key feature in intelligence. A nonlinear Schrödinger wave equation is used to model collective response behavior. It is shown that such a paradigm can naturally make a model more intelligent. This aspect has been demonstrated through an application – intelligent filtering – where complex signals are denoised without any a priori knowledge about either signal or noise. Such a paradigm has also helped us to model eye-tracking behavior. Experimental observations such as saccadic and smooth-pursuit eye-movement behavior have been successfully predicted by this model.

9.1 Intelligence – Still Ill-Understood

Natural intelligence is what determines a normal thought process of a human. Artificial intelligence is a property of a machine that gives it the ability to mimic the human thought process. The foundational framework for intelligent computing lies in our proper understanding of mental processes. Though the term *intelligence* is still not completely defined, research in artificial intelligence has focused on five components of intelligence [35], as shown in Fig. 9.1. An intelligent system should have the abilities to understand, perceive, reason, solve problems and, moreover, learn from past experiences. The understanding of cognitive processes consists of the formulation and solution of three fundamental problems in the design of intelligent machines

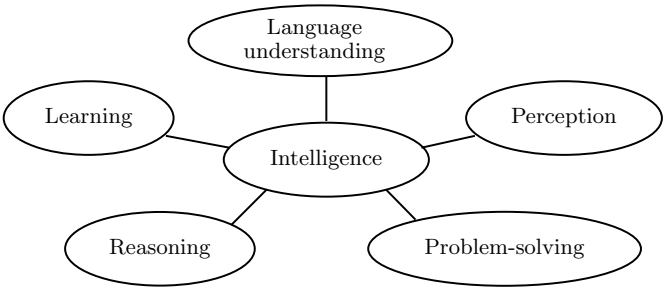

Fig. 9.1. What is intelligence? Alan Turing [35]

that "intelligently" observe, predict and interact with their surroundings. These problems are known as (i) the system-identification problem, (ii) the stochastic-filtering problem, and (iii) the adaptive-control problem.

Here we address the issue of the intelligent stochastic-filtering problem. The main question therefore is: *Can we design a method that allows us to estimate any signal embedded in noise without assuming any knowledge about the signal or noise behavior?*

Information processing in the brain is mediated by the dynamics of large, highly interconnected neuronal populations. The activity patterns exhibited by the brain are extremely rich; they include stochastic weakly correlated local firing, synchronized oscillations and bursts, and propagating waves of activity. Perception, emotion, etc., are supposed to be emergent properties of such complex nonlinear neural circuits.

Different architectures of interconnected neurons, such as feedforward and recurrent neural networks, have been explored to study global brain behavior [14, 1, 7, 8, 2]. Instead of considering one of these conventional neural architectures, an alternative neural architecture is proposed here for neural computing, namely, a recurrent quantum neural network (RQNN). This term entails that the individual neuronal response does not play a significant role when the collective behavior of a neural lattice is observed.

Population dynamics studies of "bird flocks" and "fish schools" [25] show that the individual dynamics does not play a role in group dynamics. Hence, ignoring individual neuron dynamics while considering average lattice behavior is sometimes a sound methodology. The proposed RQNN is quite different in spirit and objective from the QNN architecture available in the literature [10, 9, 32], as these QNNs synthesize a neural lattice using individual neural responses. The collective response model proposed in this chapter entails that there exists a quantum process that mediates the average behavior of a neural lattice. This collective response is described here using Schrödinger wave equation. We show that the closed-loop RQNN dynamics exhibits a soliton property. We exploit this property for stochastic filtering. The signal estimation is shown to be quite accurate. Moreover, filtering, using this approach, is done without any a priori knowledge of either signal or noise.

9.2 Intelligent Filtering – Denoising of Complex Signals

According to Bucy [13], every solution to a stochastic filtering problem involves the computation of the time-varying probability density function (pdf) on the state space of the observed system. Dawes [16, 17] proposed a novel model – a parametric avalanche stochastic filter – using this very concept. His work is the main impetus for the present work, which we hope will motivate others to explore this new approach.

For stochastic-filtering applications, we make the hypothesis that the average behavior of a neural lattice that estimates a stochastic signal is a probability density function that is mediated by a quantum process. We use the Schrödinger wave equation to track this pdf function since it is a known fact that the square of the modulus of the ψ function, the solution of this wave function, is also a pdf function. It will be explained in detail later in this chapter that the Schrödinger wave equation becomes nonlinear when its potential field is excited by a feedback signal that is a function of ψ, the state of the quantum process. It is known [11] that the nonlinear Schrödinger wave equation exhibits a soliton property, which is necessary to track nondispersing wave packets, representative of the time-varying pdf. This is a generic identity of a stochastic signal under observation.

The proposed model is an improvement over the model proposed by Dawes [17] in two respects: (i) the movement of wave packets as solitons and (ii) nonlinearly modulated spatial potential field. We also noted that it is very difficult to heuristically tune the parameters of the nonlinear Schrödinger wave equation while tracking the probability density function. This led us to make use of the evolutionary computation approach based on the univariate marginal distribution algorithm to identify these parameters in known cases of signals embedded in noise. In a recent work [6], we have shown that both Gaussian and non-Gaussian pdfs are learnt by the proposed recurrent quantum neural network (RQNN) and the signal estimation is quite accurate in the presence of a noise level up to 6 dB. The results were also compared with a classical filtering algorithm. In this work, we consider the stochastic-filtering of nonstationary signals including the speech signals. The speech-enhancement capability of the proposed RQNN is also established in real time. Thus this chapter provides a complete framework for learning a stochastic signal in terms of its probability density function.

The other important feature of our proposed model is the novelty of its application to signal processing. The popular Kalman filter assumes that the dynamic process is linear with Gaussian observation noise and the algorithm is too computationally intensive for a system of practical complexity [27]. The extended version, popularly known as EKF, makes many approximations to include nonlinear processes as well. However, in practical situations the stochastic noise can not be limited to a Gaussian or even a unimodal distribution. In contrast, the proposed RQNN estimates a signal without any a priori assumption on the shape and nature of the signal and the noise. In a nutshell, we propose a stochastic-filtering scheme that is a step forward towards intelligent filtering.

9.2.1 RQNN Architecture used for Stochastic-Filtering

The architecture of the RQNN for filtering a one-dimensional signal embedded in noise is shown in Fig. 9.2. The signal $y(t)$ is the actual signal ($y_a(t)$)

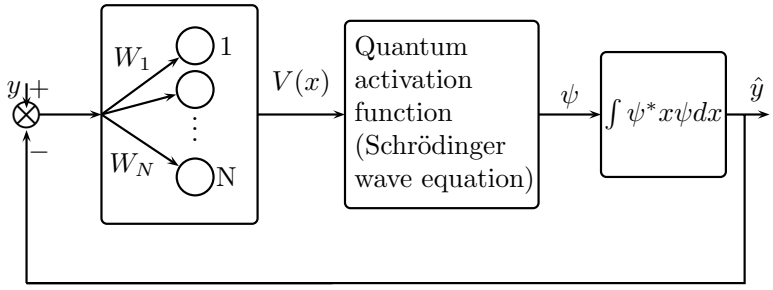

Fig. 9.2. A stochastic filter using RQNN with linear modulation

embedded in noise ($\mu(t)$), i. e. $y(t) = y_a(t) + \mu(t)$. The signal excites N neurons spatially located along the x-axis after being preprocessed by synapses. In the model the synapses are represented by time-varying synaptic weights $K(x,t)$. The unified dynamics of the one-dimensional neural lattice consisting of N neurons is described by the Schrödinger wave equation given as

$$\mathrm{i}\hbar\frac{\partial\psi(x,t)}{\partial t} = -\frac{\hbar^2}{2m}\nabla^2\psi(x,t) + \zeta(U(x,t) + G(\mid \psi \mid^2))\psi(x,t)\,, \tag{9.1}$$

where i,$\hbar, \psi(x,t)$ and ∇ carry their usual meaning in the context of Schrödinger wave equation. The $\psi(x,t)$ function represents the solution of (9.1). The potential field of the Schrödinger wave equation given in (9.1) consists of two terms:

$$U(x,t) = -K(x,t)y(t)\,, \tag{9.2}$$

$$G(\mid \psi \mid^2) = K(x,t)\int xf(x,t)\mathrm{d}x\,, \tag{9.3}$$

where

$$f(x,t) = \mid \psi(x,t) \mid^2 \ . \tag{9.4}$$

Since the potential field term in (9.1) is a function of $\psi(x,t)$, the Schrödinger wave equation that describes the stochastic filter is nonlinear. In contrast to artificial neural networks studied in the literature, in our model the neural lattice consisting of N neurons is described by the state $\psi(x,t)$ which is the solution of (9.1). Simultaneously, the model is recurrent as the dynamics consists of a feedback term $G(.)$. The information about the signal is thus transferred to the potential field of the Schrödinger wave equation and the dynamics is evolved accordingly. Here we have used a linear neural circuit to set up the potential field where $K(x,t)$s are the associated linear synaptic weights. The signal is then estimated using a maximum-likelihood estimator as

$$\hat{y}(t) = \int xf(x,t)\mathrm{d}x. \tag{9.5}$$

When the estimate $\hat{y}(t)$ is the actual signal, then the signal that generates the potential field for the Schrödinger wave equation, $\hat{\nu}(t)$, is simply the noise that is embedded in the signal. If the statistical mean of the noise is zero, then this error-correcting signal $\hat{\nu}(t)$ has little effect on the movement of the wave packet. Precisely, it is the actual signal content in the input $y(t)$ that moves the wave packet along the desired direction that, in effect, achieves the goal of the stochastic-filtering. It is expected that the synaptic weights evolve in such a manner so as to drive the ψ function to carry the exact information of the pdf of the observed stochastic variable $y(t)$.

Learning and Estimation

The nonlinear Schrödinger wave equation given by (9.1) exhibits a soliton property, i. e. the square of $\mid \psi(x,t) \mid$ is a wave packet that moves like a particle. The importance of this property is as follows. Let the stochastic variable $y(t)$ be described by a Gaussian probability density function $f(x,t)$ with mean κ and standard deviation σ. Let the initial state of (9.1) correspond to zero mean Gaussian probability density function $f'(x,t)$ with standard deviation σ'. As the dynamics evolves with online update of the synaptic weights $K(x,t)$, the probability density function $f'(x,t)$ should ideally move toward the pdf, $f(x)$ of the signal $y(t)$. Thus the filtering problem in this new framework can be seen as the ability of the nonlinear Schrödinger wave equation to produce a wave packet solution that glides along with the time-varying pdf corresponding to the signal $y(t)$.

The synaptic weights $K(x,t)$, which is a $N \times 1$-dimensional vector, is updated using the Hebbian learning algorithm

$$\frac{\partial K(x,t)}{\partial t} = \beta \nu(t) f(x,t) \,, \tag{9.6}$$

where $\nu(t) = y(t) - \hat{y}(t)$. $\hat{y}(t)$ is the filtered estimate of the actual signal $y_a(t)$. We compute the filtered estimate according to (9.5). We will show later that the wave packet moves in the required direction in our new model.

9.2.2 Integration of the Schrödinger Wave Equation

The nonlinear Schrödinger wave equation is – from the mathematical point of view – a partial differential equation with two variables: x and t. In an abstract sense, receptive fields of N neurons span the entire distance along the x-axis. (9.1) is converted into the finite difference form by dividing the x-axis into N mesh points so that x and t are represented as follows:

$$x_j = j \triangle x \quad t_n = n \triangle t \,, \tag{9.7}$$

where j varies from $-N/2$ to $+N/2$. The finite-difference form of (9.1) is expressed as

$$\mathrm{i}\frac{\psi(x,t+\triangle t)-\psi(x,t)}{\triangle t} = -\frac{\psi(x+\triangle x,t)-2\psi(x,t)+\psi(x-\triangle x,t)}{2m\triangle x^2}+V(x)\psi(x,t)\,, \quad (9.8)$$

where $V(x)=\zeta(U(x,t)+G(|\ \psi\ |^2))$. Here, we have assumed that $\hbar=1$. For convenience, we represent $\psi(x_j,t_n+\triangle t)$ as ${\psi_j}^{n+1}$, $\psi(x_j,t_n)$ as ${\psi_j}^n$ and $\psi(x_j-\triangle x,t_n)$ as ${\psi_{j-1}}^n$. With these representations, (9.8) reads

$${\psi_j}^{n+1}={\psi_j}^n+\mathrm{i}\triangle t\frac{{\psi_{j+1}}^n-2{\psi_j}^n+{\psi_{j-1}}^n}{2m\triangle x^2}-\mathrm{i}\triangle t V_j{\psi_j}^n\,. \quad (9.9)$$

Rewriting this equation in a matrix form one gets

$$F^{n+1}=F^n-\mathrm{i}\triangle t H' F^n\,, \quad (9.10)$$

where the Hamiltonian H' is defined as

$$H'=-\frac{\hbar^2}{2m}\frac{\mathrm{d}^2}{\mathrm{d}x^2}+V(x)\,. \quad (9.11)$$

Subsequently,

$$F^{n+1}=UF^n \quad \text{where} \quad U=I-\mathrm{i}\triangle t H'\,. \quad (9.12)$$

Since it is required that the norm of F is $F^*F=1$, U must be an orthonormal operator. Since U in (9.12) does not have such a property, in our simulation we impose the normalization after every step.

Selection of Parameters

The nonlinear equation (9.1) involves four external parameters: $\hbar$, m, ζ and β. The last parameter β is necessary to update the synaptic weight vector $K(x,t)$. For simplicity, the parameter $\hbar$ is taken as unity and the other three parameters are tuned accordingly. Looking at the complexity of (9.1), we used a genetic algorithm (GA) based on the concept of the univariate marginal distribution algorithm (UMDA) [5, 29] to select near-optimal parameters. The details of the algorithm and its implementation are as follows:

The univariate marginal distribution algorithm estimates the distribution of gene frequencies using a mean-field approximation. Each string in the population is represented by a binary vector $\boldsymbol{x}$. The algorithm generates new points according to the following distribution:

$$p(\boldsymbol{x},t)=\prod_{i=1}^{n}p_i^s(x_i,t)\,. \quad (9.13)$$

The UMDA algorithm is given as follows:

- Step 1: Set $t = 1$, Generate $N(>> 0)$ binary strings randomly.
- Step 2: Select $M < N$ strings according to a selection method.
- Step 3: Compute the marginal frequencies $p_i^s(x_i, t)$ from the selected strings.
- Step 4: Generate N new points according to the distribution

$$p(\boldsymbol{x}, t) = \prod_{i=1}^{n} p_i^s(x_i, t) \, .$$

- Set $t = t + 1$. If the termination criteria are not met, go to Step 2.

For infinite populations and proportionate selection, it has been shown [29] that the average fitness never decreases for the maximization problem (increases for the minimization problem).

In general, GA provided the parameter values where $m < 1, \beta < 1$ and $\zeta >> 1$. The significance of this finding can be understood in the following manner. Since β was the learning parameter in the Hebbian learning, it is natural to expect that $\beta < 1$. The less than unity value for m makes self-excitation larger. Similarly, a large value of ζ causes a larger input excitation since it appears as a multiplicand in the Schrödinger equation.

9.2.3 Simulation Results I

The proposed RQNN has been successfully applied to denoising of various signals like dc signals, sinusoids, shifted sinusoids, amplitude-modulated sine and square waves, speech signals, embedded in high Gaussian or non-Gaussian noise. Some selected results are presented in this section.

Amplitude - Modulated Sine and Square Waves

Amplitude-modulated and frequency-modulated signals are normally used in coding and transmission of data and appear corrupted at the receiver's end by channel noise [23]. For simulation purpose, we have selected the frequency of the carrier signal to be a sinusoid of frequency 5 Hz, although in reality they are very high frequency signals. The amplitude was modulated by superimposing a triangular variation of frequency 0.5 Hz. Thus the expression for the composite signal $y_a(t)$ is

$$y_a(t) = a(t) \cdot \sin(2\pi 5t) \, ; \quad a(t) = \begin{cases} 1.5t & 0 \le t \le 1 \\ 1.5\,(2-t) & 1 \le t \le 2 \, , \end{cases} \tag{9.14}$$

where $a(t)$ is periodic with period 0.5 Hz. A similar strategy is applied in generating the amplitude modulated square wave, i. e., the amplitude of $a(t)$ is kept constant over every single period of the carrier sine wave in (9.14).

The expression for the actual signal $y_a(t)$ in this case is given below:

$$y_a(t) = \begin{cases} a(t) & 0 \le t \le 0.1 \\ -a(t) & 0.1 \le t \le 0.2 \end{cases} \quad \text{and} \quad a(t) = \begin{cases} 1.5t & 0 \le t \le 1 \\ 1.5\,(2-t) & 1 \le t \le 2\,, \end{cases} \tag{9.15}$$

where $a(t)$ is periodic with period 0.5 Hz.

The amplitude-modulated sinusoid signal $y_a(t)$ in (9.14) was immersed in Gaussian noise. The variance of the Gaussian noise was set according to the 20 dB and 6 dB SNR measurement. The values selected for the parameters of the Schrödinger wave equation using UMDA are as follows:

$$\beta = 0.11 \quad m = 0.015 \quad \zeta = 84.31 \quad \hbar = 1.0\,. \tag{9.16}$$

The number of neurons along the x-axis are taken as $N = 400$. The parameters for the finite-difference equation used for integration are selected as

$$\triangle x = 0.1 \quad \triangle t = 0.001\,. \tag{9.17}$$

The parameter γ is selected as 100. The tracking of the desired signal $y_a(t)$ is shown in Fig. 9.3. It can be observed that the tracking is very smooth and accurate. Snapshots of wave packets are shown in the same figure correponding to marker points shown in the left plot. It can be observed that the pdf does not split, sliding along the x-axis back and forth like a particle. Next, the amplitude-modulated square wave $y_a(t)$ in (9.15) is immersed in Gaussian noise. The variance of the Gaussian noise was set according to the 20 dB and 6 dB noise power with the instantaneous period amplitude of $y_a(t)$

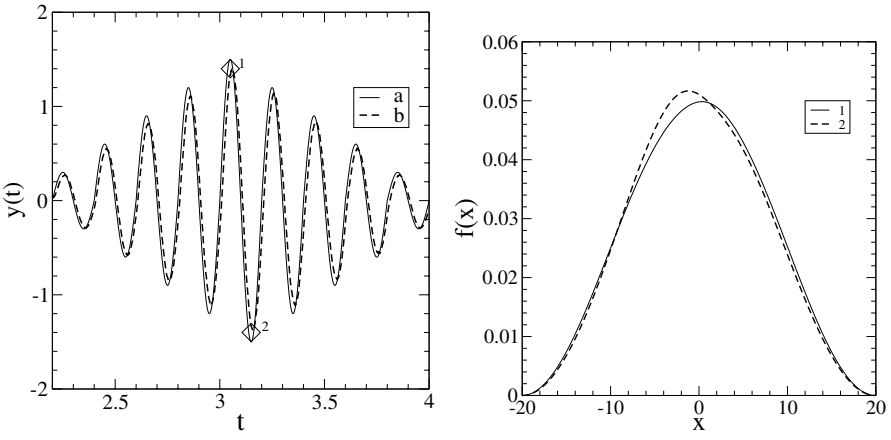

Fig. 9.3. (*left*) Tracking of amplitude-modulated sinusoid signal embedded in 20 dB Gaussian noise: "a" represents the actual signal and "b" represents the tracking by the RQNN; (*right*) Snapshots of wave packets corresponding to marker points are shown in the *left plot*

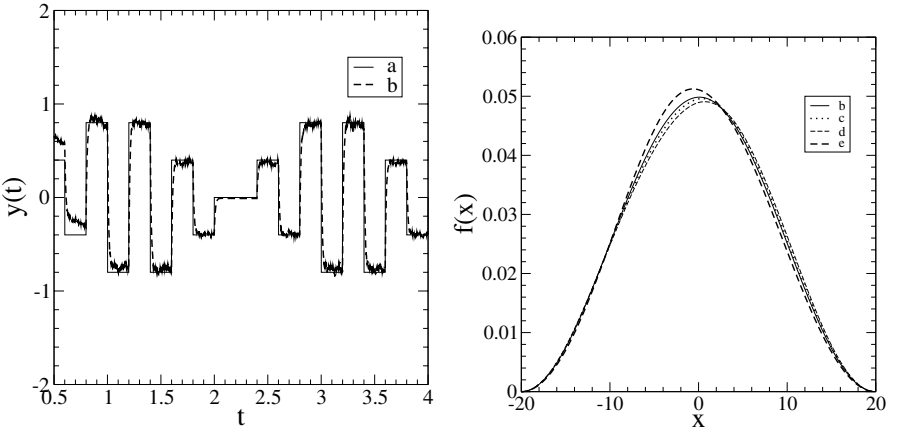

Fig. 9.4. (*left*) Tracking of amplitude-modulated square wave embedded in 20 dB Gaussian noise: "a" represents the actual signal and "b" represents the tracking by the RQNN. (*right*) Snapshots of wave packets: wave packet "b" at $t = 2.1\,s$, the wave packet "c" at $t = 2.5\,s$, wave packet "d" at $t = 2.9\,s$ and the wave packet "e" at $t = 3.1\,s$

as reference. The values selected for the parameters of the Schrödinger wave equation using UMDA are as follows:

$$\beta = 0.11 \quad m = 0.015 \quad \zeta = 84.31 \quad \hbar = 1.0\,. \tag{9.18}$$

This shows that the parameter γ influences the speed of response of the RQNN filter. The number of neurons along the x-axis is taken as $N = 400$. The parameters for the finite-difference equation used for integration are selected as

$$\triangle x = 0.1 \quad \triangle t = 0.001\,. \tag{9.19}$$

The tracking of the desired signal $y_a(t)$ and the movement of the wave packets are shown in Fig. 9.4. It can be observed that the tracking is accurate.

The pdf of the desired signal as estimated by the RQNN clearly exhibits a soliton property Fig. 9.4. The pdf does not split and slides along the x-axis like a particle.

Speech Signals

Speech signals are degraded in many ways that limit their effectiveness for communication. One major source of noise in the speech signal is *channel noise* that is a major concern, especially in speech-recognition systems. Since the RQNN estimates the pdf of the incoming signal at every instant, if the incoming signal is corrupted by zero-mean noise, then the RQNN must be able to filter out that noise. Working on this hypothesis, we added zero-mean Gaussian noise with variance equal to the square of the instantaneous

amplitude of the speech signal. The peak amplitude of the speech signal was normalized to 1.0. The original speech signals are recorded spoken digit utterances taken from the Release 1.0 of the Number Corpus. This corpus is distributed by the Center of Spoken Language Understanding of the Oregon Graduate Institute. The speech file names are mentioned in the captions, along with the respective plots for each of the speech signals.

For tracking the speech signals, the number of neurons along the x-axis is taken as $N = 400$. The parameters for the finite-difference equation used for integration are selected as

$$\triangle x = 0.1 \quad \triangle t = 0.001\,. \tag{9.20}$$

The values selected for the parameters of the Schrödinger wave equation using UMDA are as follows:

$$\beta = 0.16 \quad m = 0.015 \quad \zeta = 27.45 \quad \hbar = 1.0. \tag{9.21}$$

The parameter γ was selected as 800. The tracking for a particular period of the speech signals selected from the database are shown in Figs. 9.5 and 9.6. The snapshots of the wave packet at two time instants are also shown. It is evident from Figs. 9.5 and 9.6 that the RQNN does track the pdf of the input signal at every instant. The wave packet does not split and it maintains an approximate Gaussian nature. It moves slightly along the x-axis like a particle maintaining its soliton property. By estimating the actual signal as the mean of the pdf at every instant, we can filter out the corrupting noise added to the actual signal. In addition, we reconverted the tracked speech signal and the noisy speech signal to the *WAV* format. On listening to these signals, we

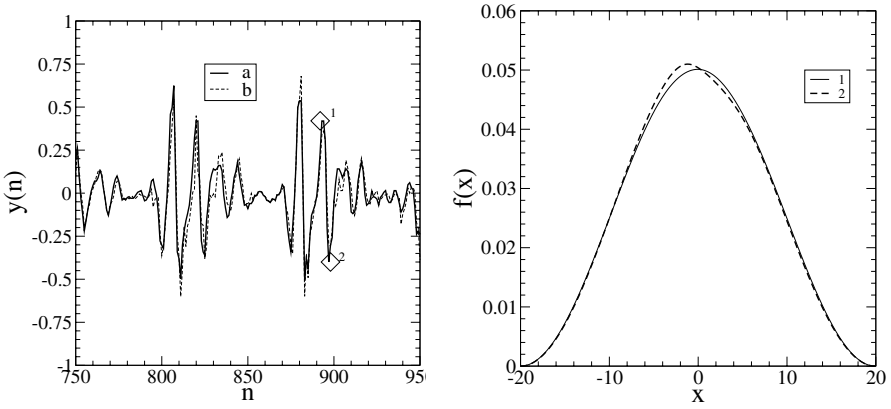

Fig. 9.5. Speech file NU_24streetaddr.wav: *(left)* Filtering of speech signal immersed in Gaussian noise: "a" represents the actual speech signal and "b" represents the tracking by the RQNN; *(right)* Snapshots of wave packets at marker points (1,2) shown in the *left plot*

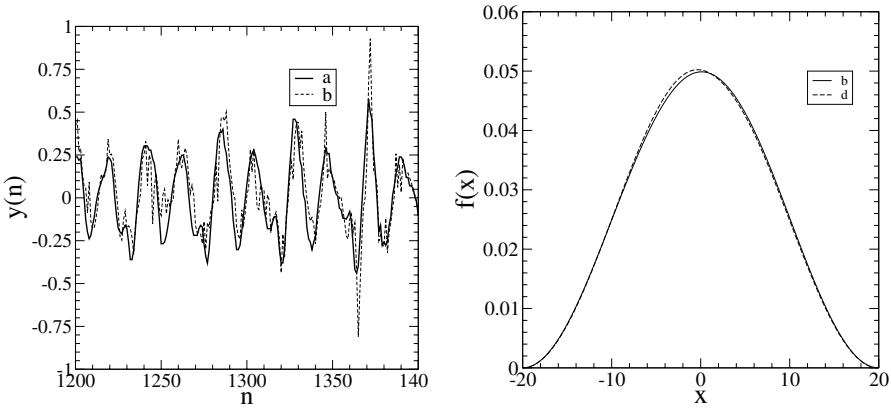

Fig. 9.6. (*left*) Filtering of speech signal immersed in Gaussian noise: "a" represents the actual speech signal and "b" represents the tracking by the RQNN. The x-axis represents the sample number n of the speech signal. (*right*) Movement of the wave packet: wave packet "b" at $t = 1.35\,s$ and wave packet "d" at $t = 1.45\,s$

could verify that the RQNN filtering does improve the quality of the input noisy speech signal if corrupted by zero-mean Gaussian noise.

9.3 A Comprehensive Quantum Model of Intelligent Behavior

Biological organisms perform many complex tasks with ease. Although we may have supercomputers that have reached the level of computing power beyond our imagination, some of the tasks we perform, such as pattern recognition and language undrstanding, are still beyond the reach of such supercomputers. Can quantum-mechanical models better account for such complex behavior in biological organisms? The rest of this chapter is devoted to this question. We propose a theoretical quantum brain model to explain human eye movement behavior, where the same collective response attribute of natural intelligence plays the key role. While simulating the quantum brain model, two very interesting phenomena are observed. First, as eye-sensor data is processed in a classical brain, a wave packet is triggered in the quantum brain. This wave packet moves like a particle. Secondly, when the eye tracks a fixed target, this wave packet moves not in a continuous but rather in a discrete mode. This result reminds one of the saccadic movements of the eye consisting of "jumps" and "rests". However, such a saccadic movement is intertwined with smooth-pursuit movements when the eye has to track a dynamic trajectory. In this sense, the proposed quantum brain concept is very successful in explaining the nature of eye movements that also accord with the experimental observations.

9.4 RQNN-based Eye-Tracking Model

There are certain aspects of brain functions that still appear to have no satisfactory explanation. As an alternative, researchers [36, 37, 21, 28] are investigating whether the brain can demonstrate quantum-mechanical behavior. According to a current hypothesis, microtubules, the basic components of neural cytoskeleton, are very likely to possess quantum-mechanical properties due to their size and structure. The tubulin protein, which is the structural block of microtubules, has the ability to flip from one conformation to another as a result of a shift in the electron-density localization from one resonance orbital to another. These two conformations act as two basis states of the system according to whether the electrons inside the tubuline hydrophobic pocket are localized closer to α or β tubulin. Moreover, the system can lie in a superposition of these two basis states, that is, being in both states simultaneously, which can give a plausible mechanism for creating a coherent state in the brain. Penrose [30] therefore argued that the human brain must utilize quantum-mechanical effects when demonstrating problem solving feats that cannot be explained algorithmically.

In this chapter, instead of going into the biological details of the brain, we propose a theoretical quantum brain model using the RQNN. The RQNN model proposed in Sect. 9.2.1 has been modified a little to cope with the present application. Instead of using a linear neural circuit to set up the potential field in which the quantum brain is dynamically excited, the present model uses a nonlinear neural circuit. This fundamental change in the architecture has yielded two novel features. The wave packets, $f(x,t) =\mid \psi(x,t) \mid^2$, are moving like particles. Here $\psi(x,t)$ is the solution of the nonlinear Schrödinger wave equation that describes the proposed quantum brain model to explain eye movements for tracking moving targets. The other very interesting observation is that the movements of the wave packets, while tracking a fixed target, are not continuous but discrete. These observations accord with the well-known saccadic movement of the eye [3, 18]. In a way, our model is the first of its kind to explain the nature of eye movements in static scenes that consists of "jumps" (saccades) and "rests" (fixations). We expect this result to inspire other researchers to further investigate the possible quantum dynamics of the brain.

9.4.1 A Theoretical Quantum Brain Model

An impetus to hypothesize a quantum brain model comes from the brain's necessity to unify the neuronal response into a single percept. Anatomical, neurophysiological and neuropsychological evidences, as well as brain imaging using fMRI and PET scans, show that separate functional MAPs exist in the brain to code separate features such as direction of motion, location, color and orientation. How does the brain compute all these data to have a coherent perception? Here, a very simple model of a quantum brain is proposed, where

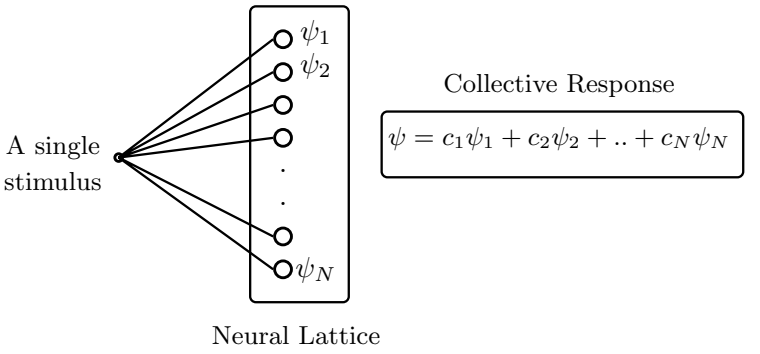

Fig. 9.7. Quantum brain – a theoretical model

a collective response of a neuronal lattice is modeled using a Schrödinger wave equation as shown in Fig. 9.7.

In this figure, it is shown that an external stimulus reaches each neuron in a lattice with a probability amplitude function ψ_i. This hypothesis suggests that the carrier of the stimulus performs quantum computation. The collective response of all the neurons is given by the superposition

$$\psi = c_1\psi_1 + c_2\psi_2 + \cdots + c_N\psi_N = \sum_{i=1}^{N} c_i\psi_i \, . \tag{9.22}$$

We suggest that the time evolution of the collective response ψ is described by the Schrödinger wave equation

$$\mathrm{i}\hbar\frac{\partial\psi(x,t)}{\partial t} = -\frac{\hbar^2}{2m}\nabla^2\psi(x,t) + V(x)\psi(x,t) \, , \tag{9.23}$$

where $2\pi\hbar$ is Planck's constant, $\psi(x,t)$ is the wave function (probability amplitude) associated with the quantum object at space–time point (x,t), and m the mass of the quantum object. Further symbols such as i and ∇ carry their usual meaning in the context of the Schrödinger wave equation. Another way to look at our proposed quantum brain is as follows. A neuronal lattice sets up a spatial potential field $V(x)$. A quantum process described by a quantum state ψ, which mediates the collective response of a neuronal lattice, evolves in the spatial potential field $V(x)$ according to (9.23). Thus the classical brain sets up a spatiotemporal potential field, while the quantum brain is excited by this potential field to provide a collective response.

9.4.2 An Eye–Tracking Model using RQNN with Nonlinear Modulation of Potential Field

In this section we present an extension of RQNN, briefly described in the previous section. Here, the potential field of the Schrödinger wave equation is

modulated using a nonlinear neural circuit that results in a much pronounced soliton behavior of the wave packet. With this modification we now provide a plausible biological mechanism for eye tracking using the quantum brain model proposed in Sect. 9.4.1. The mechanism of eye movements, tracking a moving target consists of three stages as shown in Fig. 9.8: (i) stochastic-filtering of noisy data that impact the eye sensors; (ii) a predictor that predicts the next spatial position of the moving target; and (iii) a biological motor control system that aligns the eye pupil along the moving targets trajectory. The biological eye sensor fans out the input signal y to a specific neural lattice in the visual cortex. For clarity, Fig. 9.8 shows a one-dimensional array of neurons whose receptive fields are excited by the signal input y reaching each neuron through a synaptic connection described by a nonlinear MAP. The neural lattice responds to the stimulus by setting up a spatial potential field, $V(x,t)$, which is a function of external stimulus y and estimated trajectory $\hat{y}$ of the moving target:

$$V(x,t) = \sum_{i=1}^{n} W_i(x,t)\phi_i(\nu(t)) \,, \tag{9.24}$$

where $\phi_i(.)$ is a Gaussian kernel function, n represents the number of such Gaussian functions describing the nonlinear MAP that represents the synaptic connections, $\nu(t)$ represents the difference between y and $\hat{y}$ and W represents the synaptic weights as shown in Fig. 9.8. The Gaussian kernel function is taken as

$$\phi_i(\nu(t)) = \exp(-(\nu(t) - g_i)^2) \,, \tag{9.25}$$

where g_i is the center of the i-th Gaussian function, ϕ_i. This center is chosen from input space described by the input signal, $\nu(t)$, through uniform random sampling.

Our quantum-brain model proposes that a quantum process mediates the collective response of this neuronal lattice that sets up a spatial potential field $V(x,t)$. This happens when the quantum state associated with this quantum

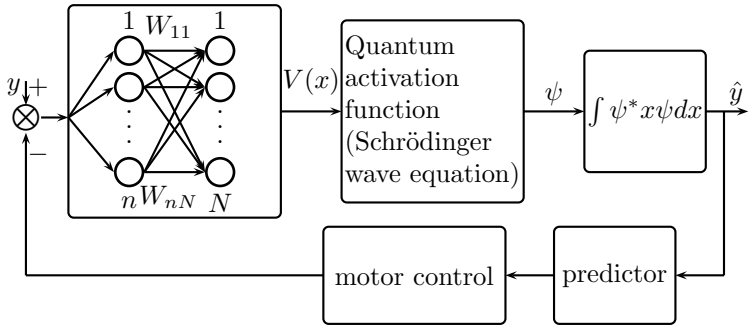

Fig. 9.8. Eye tracking-model using RQNN

process evolves in this potential field. The spatiotemporal evolution follows as per (9.23). *We hypothesize that this collective response is described by a wave packet,* $f(x,t) =\mid \psi(x,t) \mid^2$*, where the term* $\psi(x,t)$ *represents a quantum state.* In a generic sense, we assume that a classical stimulus in a brain triggers a wave packet in the counterpart "*quantum brain*". This subjective response, $f(x,t)$, is quantified using the following estimate equation:

$$\hat{y}(t) = \int x(t) f(x,t) \mathrm{d}x \, . \tag{9.26}$$

The estimate equation is motivated by the fact that the wave packet, $f(x,t) =\mid \psi(x,t) \mid^2$ is interpreted as the probability density function. Although computation of (9.26) using the nonlinear Schrödinger wave equation is straightforward, we hypothesize that this computation can be done through an interaction between a quantum and a classical brain, using a suitable quantum measurement operator. At this point we will not speculate about the nature of such a quantum measurement operator that will estimate the ψ function necessary to compute (9.26). Based on this estimate, $\hat{y}$, the predictor estimates the next spatial position of the moving target. To simplify our analysis, the predictor is made silent. Thus its output is the same as that of $\hat{y}$. The biological motor control is commanded to fixate the eye pupil to align with the target position, which is predicted to be at $\hat{y}$. Obviously, we have assumed that biological motor control is ideal.

After the above-mentioned simplification, the closed form dynamics of the model described by Fig. 9.8 becomes

$$\mathrm{i}\hbar \frac{\partial \psi(x,t)}{\partial t} = -\frac{\hbar^2}{2m} \nabla^2 \psi(x,t) + \zeta G \left(y(t) - \int x \mid \psi(x,t) \mid^2 \mathrm{d}x \right), \psi(x,t) \, , \tag{9.27}$$

where $G(.)$ is a Gaussian kernel MAP introduced to nonlinearly modulate the spatial potential field that excites the dynamics of the quantum object. In fact, $\zeta G(.) = V(x,t)$, where $V(x,t)$ is given in (9.24).

The nonlinear Schrödinger wave equation given by (9.27) is one-dimensional with cubic nonlinearity. Interestingly, the closed-form dynamics of the recurrent quantum neural network (equation (9.27)) closely resembles a nonlinear Schrödinger wave equation with cubic nonlinearity studied in quantum electrodynamics [20]:

$$\mathrm{i}\hbar \frac{\partial \psi(x,t)}{\partial t} = \left(-\frac{\hbar^2}{2m} \nabla^2 - \frac{e^2}{r} \right) \psi(x,t) + e^2 \int \frac{\psi(x,t) \mid \psi(x',t) \mid^2}{\mid x - x' \mid} \mathrm{d}x' \, , \tag{9.28}$$

where m is the electron mass, e the elementary charge and r the magnitude of $\mid x \mid$. Also, nonlinear Schrödinger wave equations with cubic nonlinearity of the form $\frac{\partial}{\partial t}\mathcal{A}(t) = c_1 \mathcal{A} + c_3 \mid \mathcal{A} \mid^2 \mathcal{A}$, where c_1 and c_3 are constants, frequently appear in nonlinear optics [12] and in the study of solitons [24, 11, 15, 33]. Application of the nonlinear Schrödinger wave equation for the study of quantum systems can also be found in [34].

In (9.27), the unknown parameters are weights $W_i(x,t)$ associated with the Gaussian kernel, mass m, and ζ, the scaling factor to actuate the spatial potential field. The weights are updated using the Hebbian learning algorithm

$$\frac{\partial W_i(x,t)}{\partial t} = \beta \phi_i(\nu(t)) f(x,t) \,, \tag{9.29}$$

where $\nu(t) = y(t) - \hat{y}(t)$.

The idea behind the proposed quantum computing model is as follows. As an individual observes a moving target, the uncertian spatial position of the moving target triggers a wave packet within the quantum brain. The quantum brain is so hypothesized that this wave packet turns out to be a collective response of a classical neural lattice. As we combine (9.27) and (9.29), it is desired that there exist some parameters m, ζ and β such that each specific spatial position $x(t)$ triggers a unique wave packet, $f(x,t) =\mid \psi(x,t) \mid^2$, in the quantum brain. This brings us to the question of whether the closed form dynamics can exhibit soliton properties that are desirable for target tracking. As pointed out above, our equation has a form that is known to possess soliton properties for a certain range of parameters and we just have to find those parameters for each specific problem.

We would like to reiterate the importance of the soliton properties. According to our model, eye tracking means tracking of a wave packet in the domain of the quantum brain. The biological motor control aligns the eye pupil along the spatial position of the external target that the eye tracks. As the eye sensor receives data y from this position, the resulting error stimulates the quantum brain. In a noisy background, if the tracking is accurate, then this error-correcting signal $\nu(t)$ has little effect on the movement of the wave packet. Precisely, it is the actual signal content in the input $y(t)$ that moves the wave packet along the desired direction that, in effect, achieves the goal of the stochastic filtering part of the eye movement for tracking purposes.

9.4.3 Simulation Results II

In this section we present simulation results to test target tracking through eye movement where targets are either fixed or moving.

For fixed target tracking, we have simulated a stochastic-filtering problem of a dc signal embedded in Gaussian noise. As the eye tracks a fixed target, the corresponding dc signal is taken as $y_a(t) = 2.0$, embedded in Gaussian noise with SNR (signal-to-noise ratio) values of 20 dB, 6 dB and 0 dB.

We next compared the results with the performance of a Kalman filter [19] designed for this purpose. It should be noted that the operation of the Kalman filter is based on a priori information that the embedded signal is a dc signal, whereas the RQNN is not provided with this information. The Kalman filter also makes use of the fact that the noise is Gaussian and estimates the variance of the noise based on this assumption. Thus it is expected

that the performance of the Kalman filter will degrade as the noise becomes non-Gaussian. In contrast, the RQNN model does not make any assumption about the noise.

Notice that there are certain values of β, m, ζ and N for which the model performs optimally. A univariate marginal distribution algorithm was used to get near optimal parameters while fixing $N = 400$ and $\hbar = 1.0$. The selected values of these parameters are as follows for all levels of SNR:

$$\beta = 0.86; \quad m = 2.5; \quad \zeta = 2000. \tag{9.30}$$

The comparative performance of eye tracking in terms of rms error for all the noise levels is shown in Table 9.1. It is easily seen from Table 9.1 that the rms tracking error of RQNN is much less than that of the Kalman filter. Moreover, RQNN performs equally well for all the three categories of noise levels, whereas the performance of the Kalman filter degrades with the increase in noise level. In this sense we can say that our model performs the tracking with a greater efficiency compared to the Kalman filter. The exact nature of trajectory tracking is shown for 0 dB SNR in Fig. 9.9. In this figure, the noise envelope is shown, and obviously its size is large due to a high noise content in the signal. The figure shows the trajectory of the eye movement as the eye focuses on a fixed target.

To better appreciate the tracking performance, an error plot is shown in Fig. 9.10. Although Kalman-filter tracking is continuous, the RQNN model tracking consists of "jumps" and "fixations". As the alignment of the eye pupil becomes closer to the target position, the "fixation" time also increases. Similar tracking behavior was also observed for the SNR values of 20 and 6 dB.

These theoretical results are very interesting when compared to experimental results in the field of eye-tracking. In eye-tracking experiments, it is known that eye movements in static scenes are not performed continuously, but consist of "jumps" (saccades) and "rests" (fixations). Eye-tracking results are represented as lists of fixation data. Furthermore, if the information is simple or familiar, eye movement is comparatively smooth. If it is tricky or new, the eye might pause or even flip back and forth between images. Similar results are given by our simulations. Our model tracks the dc signal that can be thought of as equivalent to a static scene, in discrete steps rather than in

Table 9.1. Performance comparison between Kalman filter and RQNN for various levels of Gaussian noise

Noise level in dB	RMS error for Kalman filter	RMS error for RQNN
20	0.0018	0.000040
6	0.0270	0.000062
0	0.0880	0.000090

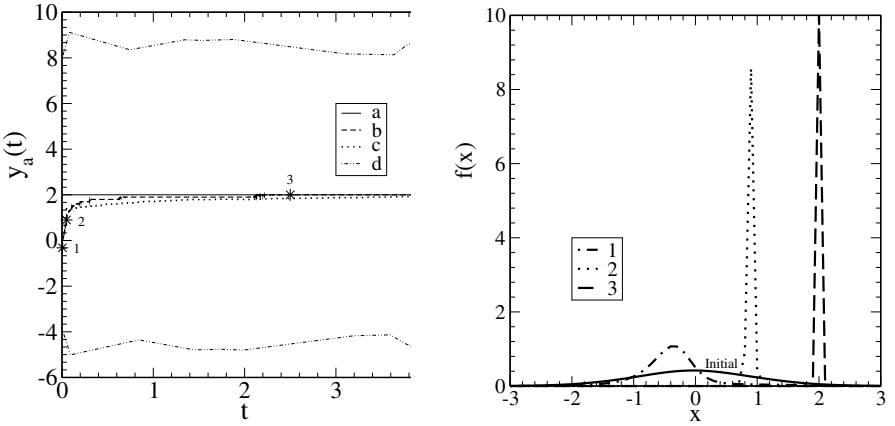

Fig. 9.9. (*left*) Eye tracking of a fixed target in a noisy environment of 0 dB SNR: "a" respresents fixed target, "b" represents target tracking using RQNN model and "c" represents target tracking using a Kalman filter. The noise envelope is represented by the curve "d"; (*right*) The snapshots of the wave packets at different instances corresponding to the marker points (1,2,3) as shown in the *left figure*. The solid line represent the initial wave packet assigned to the Schrödinger wave equation

a continuous fashion. This is very clearly understood from the tracking error in Fig. 9.10.

The other interesting aspect of the results is the movement of wave packets. It is observed that these wave packets move in discrete steps, i. e. the movement is not continuous. In Fig. 9.9 (*right*), snapshots of wave packets

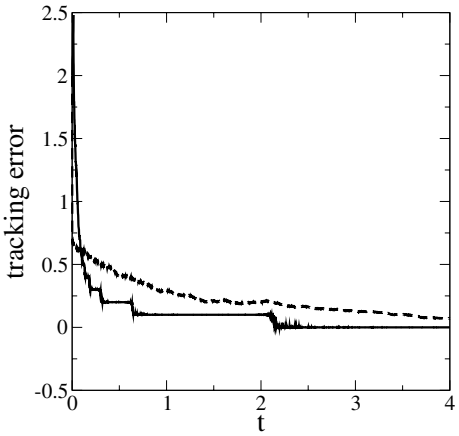

Fig. 9.10. The continuous line represents the tracking error using RQNN model, while the broken line represents the tracking error using a Kalman filter

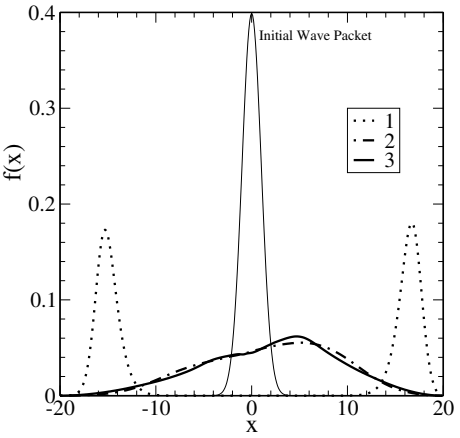

Fig. 9.11. Wave-packet movements for RQNN with linear weights

are plotted at different instances corresponding to marker points as shown along the desired trajectory. It can be noticed that a very flat initial Gaussian wave packet first moves to the left, and then proceeds toward the right until the mean of the wave packet exactly matches the actual spatial position. A similar pattern of movement of wave packets was also noticed in the case of 20 and 6 dB SNR. The wave-packet movement is compared with the same, when instead of nonlinear modulation of the potential field, we use a linear modulation as described in Sect. 9.2.1 in Fig. 9.11. The initial wave packet in the previous model first splits into two parts, then moves in a continuous fashion, ultimately going into a state with a mean of approximately 2 but with high variance. In contrast, in the present model there is no splitting of the wave packet, movement is discrete and variance is also much smaller. Thus the soliton behavior of the present model is highly pronounced.

To analyze the eye movement following a moving target, a sinusoidal signal $y_a(t) = 2\sin 2\pi 10t$ is taken as the desired dynamic trajectory. This signal is embedded in 20 dB Gaussian noise. The parameter values for tracking this signal were fixed at $\beta = 0.01, m = 1.75$ and $\zeta = -250$. It is observed that during the training phase, the wave packet jumps from time to time, thus changing the tracking error in steps until a steady-state trajectory following is achieved.

This feature can be better understood from the tracking-error plot that is shown in Fig. 9.12. In this figure we have plotted the tracking error between the actual sinusoidal signal and the predicted signal using the estimate (9.26). It is clearly seen that in the first stage of tracking, the error is fluctuating very frequently between its local maximum and minimum values in the negative region. Then this fluctuation settles down in the second stage. In the third stage this fluctuation starts again and the error is flipping between the local maxima and minima in the positive region. As the estimation (see (9.26)) of

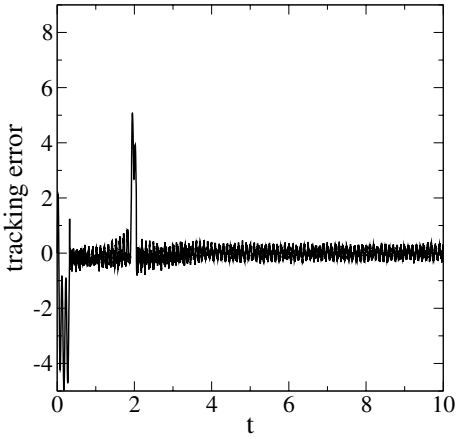

Fig. 9.12. Saccadic and pursuit movement of eye during dynamic trajectory following

the signal is very much dependent on the nature of the wave packet, the error dynamics is also correlated with the wave-packet movement. Discontinuities in error are reflected in the movement of the wave packet. It is obvious that the position of the wave packet is changing very frequently in the first stage, thus changing the mean value correspondingly, and it has no connection with the signal mean value. This means that there are a number of discontinuties or "jumps" in the wave-packet movement in the first stage. Then, in the second stage the movement becomes continuous with the mean values following the signal mean values. Again in the third stage the discontinuties take place several times, ultimately achieving a steady-state movement in the last stage.

Once a steady state is achieved, the tracking is efficient and the wave-packet movement is continuous, as shown in Fig. 9.13. In this figure, the snapshots of wave packets are plotted for three different instances of time indicated by the marker points (1,2,3) as shown in the trajectory tracking. When the signal is at position 1, the corresponding wave packet has a mean at 0. When the signal is at position 2, the corresponding wave packet has a mean at +2, and the mean of the wave packet moves to –2 when the signal goes to position 3. As seen in Fig. 9.13, during the continuous movement of the wave packets, trajectory tracking is smooth, which is similar to smooth-pursuit movement of biological eye tracking. Smooth pursuit is the eye movement that smoothly tracks slowly moving targets in the visual field. The purpose of smooth pursuit is partly to stabilize moving targets on the retina. It is a much slower movement than saccades. Eye-tracking experiments reveal that when pursuing a moving target, the smooth eye movements generally have a gain less than unity. The errors introduced by this are corrected by saccades that bring the target back on the fovea. Thus after one or two quick saccades to capture the target, the eye movement attains a steady-state velocity that

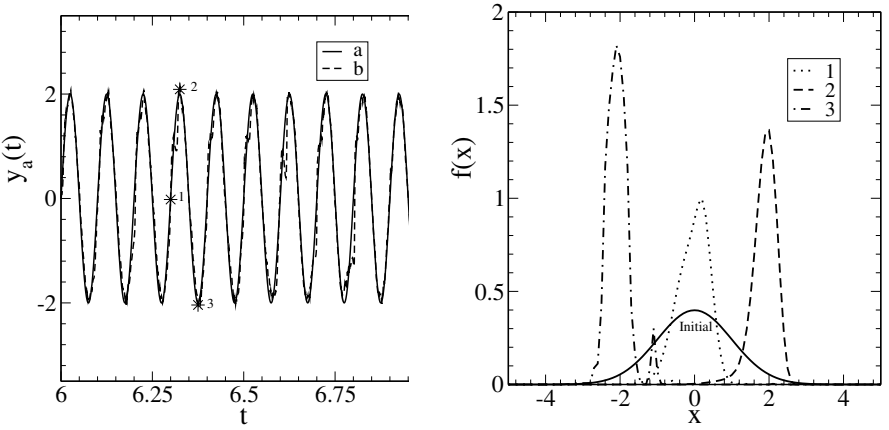

Fig. 9.13. (*left*) Eye tracking of a moving target in a noisy environment of 20 dB SNR: "a" respresents a moving target, "b" represents target tracking using RQNN model; (*right*) The snapshots of the wave packets at different instances corresponding to the marker points (1,2,3) are shown in the figure. The solid line represents the initial wave packet assigned to the Schrödinger wave equation

matches the velocity of the target. In other words, during visual tracking of a moving object, saccadic and smooth-pursuit eye movements combine to keep the target image close to the fovea [26, 31]. This kind of movement is also called dual-mode tracking [4]. This experimental result completely agrees with the obeservation when our theoretical model tracks a smoothly varying trajectory.

9.5 Concluding Remarks

We presented an alternative neural information-processing architecture where a quantum process mediates the collective response of a neural lattice having spatial structure. The key feature of this model is *collective response behavior* that is identified as an attribute of intelligent behavior. The proposed RQNN is governed by a single-dimensional nonlinear Schrödinger wave equation. The nonlinear Schrödinger wave equation that emerged due to recurrent structure of the network exhibits soliton property – a property that defines the particle type of movement of the wave packet. Two types of RQNN-based applications have been considered here. The first application makes a model naturally more intelligent. In this application, complex signals such as amplitude-modulated signals and speech signals are denoised without making any assumption about the signal and noise as well. In contrast, all prevalent techniques use a priori information about the signal and noise before signals can be denoised.

The second application is a quantum brain model of eye tracking. The key concept here is that quantum-based models can be more predictive to explain complex biological phenomena such as eye-movement behavior. The interesting finding is that our theoretical model of eye tracking agrees with previously observed experimental results. The model predicts that eye movements will be of saccadic type while following a static trajectory. In the case of a dynamic trajectory, the eye movement consists of saccades and smooth pursuits. In this sense, the proposed quantum brain concept is very successful in explaining the nature of eye movements. Earlier explanations [3] for saccadic movement have been primarily attributed to a motor control mechanism, whereas the present model emphasizes that such eye movements are due to a decision-making process of the brain – albeit a quantum brain. Thus the contribution of this chapter for the explanation of biological eye movement as a neural information-processing event may inspire researchers to study quantum brain models from the biological perspective.

The other significant contribution is the prediction efficiency of the proposed model over the prevailing model. The stochastic-filtering of a dc signal using RQNN is 1000 times more accurate compared to a Kalman filter.

At this point we are silent about the exact biological connection between the classical and the quantum brain, as it is not clear to us. The model just assumes that the quantum brain is excited by the potential field set up by the classical brain. Another obvious question is that of decoherence. In this regard, we admit that the model proposed here is highly idealized since we have used the Schrödinger wave equation. In our future work we intend to replace the Schrödinger wave equation by a density matrix approach. Also, the phase-transition analysis of closed form dynamics, given in (9.27) with respect to various parameters m, ζ, β and N, has been kept for future work.

Finally, we believe that apart from the computational power derived from quantum computing, quantum learning systems may also provide a potent framework to study the subjective aspects of the nervous system [22]. The challenge to bridge the gap between physical and mental (or objective and subjective) aspects of matter may be most successfully met within the framework of quantum learning systems. In this framework, we have proposed a notion of a quantum brain, and a recurrent quantum neural network has been hypothesized as a first step towards a neural computing model.

References

1. Amari, S. (1983). *IEEE Trans SMC*, **SMC-13(5)**:741–748.
2. Amit, D.J. (1989). *Modeling Brain Function*. Springer-Verlag, Berlin/Heidelberg.
3. Bahill, A.T. and Stark, L. (1979). *Scientific American* **240**:84–93.
4. Bahill, A.T., Iandolo, M.J., and Troost, B.T. (1980). *Vision Research*, **20**:923–931.

5. Behera, L. (2002). *New Optimization Techniques in Engineering*, chapter Parametric Optimization of a Fuzzy Logic Controller for Nonlinear Dynamical Systems using Evolutionary Computation. McGraw-Hill. New York.
6. Behera, L. and Sundaram, B. (2004). *Proceedings, International Conference on Intelligent Sensors and Information Processing*.
7. Behera, L., Gopal, M., and Chaudhury, S. (1996). *IEEE Trans Neural Networks*, **7(6)**:1401–1414.
8. Behera, L., Chaudhury, S., and Gopal, M. (1998). *IEE Proceedings Control Theory and Applications*, **145(2)**:134–140.
9. Behrman, E.C., Chandrashekar, V., Wang, Z., Belur, C.K., Steck, J.E., and Skinner, S.R. (2002). *Physical Review Letters*. Submitted.
10. Behrman, E.C., Nash, L.R., Steck, J.E., Chandrashekar, V.G., and Skinner, S.R. (2000). *Information Sciences*, **128(3–4)**:257–269.
11. Bialynicki-Birula, I. and Mycielski, J. (1976). *Annals of Physics*, **100**:62–93.
12. Boyd, R.W. (1991). *Nonlinear Optics*. Academic Press. London.
13. Bucy, R.S. (1970). *IEEE Proceedings*, **58(6)**:854–864.
14. Cohen, M.A. and Grossberg, S. (1983). *IEEE Trans Syst, Man and Cybernetics*, **13**:815–826.
15. Davydov, A.S. (1982). *Biology and Quantum Mechanics*. Pergamon Press, Oxford.
16. Dawes, R.L. (1992). *IJCNN Proceedings*, 133.
17. Dawes, R.L. (1993). *Rethinking Neural Networks: Quantum Fields and Biological Data*, chapter – Advances in the theory of quantum neurodynamics. Erlbaum, Hillsdale, N.J.
18. Findlay, J.M. Brown, V., and Gilchrist, I.D. (2001). *Vision Research*, **41**:87–95.
19. Grewal, M.S. and Andrews, A.P. (2001). *Kalman Filtering: Theory and Practice Using MATLAB*. Wiley-Interscience. USA.
20. Gupta, S. and Zia, R.K.P. (2001). *Journal of Computer and System Sciences*, **63(3)**:355–383.
21. Hagan, S., Hameroff, S.R., and Tuszynski, J.A. (2002). *Physical Review E*, **65**:061901.
22. Atmanspacher, H. (2004). *Discrete Dynamics*, **8**:51–73.
23. Haykin, S. (2001). *Communication Systems*. John Wiley and Sons, Inc., 4th edn. New York.
24. Jackson, E. Atlee (1991). *Perspectives of Nonlinear Dynamics*. Cambridge. Cambridge University Press.
25. Kennedy, J. and Eberhart, R.C. (2001). *Swarm Intelligence*. Morgan Kauffman. USA.
26. Leung, H. and Kettner, R.E. (1997). *Vision Research*, **37(10)**:1347–1354.
27. Mendel, J.M. (1971). *IEEE Trans Automatic Control*, **AC-16**:748–758.
28. Mershin, A., Nanopoulos, D.V., and Skoulakis, E. (1999). *Proc. Acad. Athens*, **74**:148–179.
29. Muehlenbein, H. and Thilo Mahnig. (2001). *Foundations of Real-World Intelligence*, chapter – Evolutionary Computation and Beyond. CSLI Publications. Stanford.
30. Penrose, R. (1994). *Shadows of the Mind*. Oxford University Press. Oxford.
31. Pola, J., and Wyatt, H.J. (1997). *Vision Research*, **37(18)**:2579–2595.

32. Purushothaman, G. and Karayiannis, N.B. (1997). *IEEE Tran. on Neural Networks*, **8(3)**:679–693.
33. Scott, A.C., Chu, F.Y.F., and McLaughlin, D.W. (1973). *IEEE Proceedings*, **61(10)**:1443–1483.
34. Sulem, C., Sulem, P.L., and Sulem, C. (1999). *Nonlinear Schrödinger Equations: Self-Focusing and Wave Collapse*. Springer-Verlag. (Applied Mathematical Sciences/139). New York.
35. Turing, A.M. (1950). *Mind*, **59**:433–460.
36. Tuszynski, J.A., Hameroff, S.R., Sataric, M.V., Trpisova, B., and Nip, M.L.A. (1995). *Journal of Theoretical Biology*, **174**:371–380.
37. Vitiello, G. (1995). *International Journal of Modern Physics B*, **9**:973–989.